J. Fluid Mech. (2008), *vol.* 598, *pp.* 107–119. © 2008 Cambridge University Press
doi:10.1017/S0022112007009731 Printed in the United Kingdom

Landslide tsunamis propagating along a plane beach

P. SAMMARCO AND E. RENZI

Dipartimento di Ingegneria Civile, Università degli Studi di Roma Tor Vergata, Via del Politecnico 1, 00133, Roma, Italy

(Received 12 June 2007 and in revised form 14 November 2007)

A forced two-horizontal-dimension analytical model is developed to investigate the distinguishing physical features of landslide-induced tsunamis generated and propagating on a plane beach. The analytical solution is employed to study the wave field at small times after the landslide motion starts. At larger times, the occurrence of transient edge waves travelling along the shoreline is demonstrated, showing the differences with the transient waves propagating over a bottom of constant depth. Results are satisfactorily compared with available experimental data. Finally, the validity of non-forced numerical models is discussed.

1. Introduction

Landslide tsunamis occur as a consequence of local events, and are characterized by a length scale $O(1\text{ km})$, much smaller than that of earthquake-generated tsunamis, $O(100\text{ km})$, though the maximum induced runup can be still significant. The first systematic experiments on landslide tsunami generation, by Wiegel (1955) with sliding blocks down an incline, showed that the induced wave height increases with increasing the slope, while decreasing with increasing submergence of the sliding mass. More recently, Watts (1997) performed a series of similar tests on a smaller scale with sliding blocks, though concentrating on the block terminal velocity and not measuring wave runup. Large-scale experiments of Liu *et al.* (2005) investigated the correlation between the maximum runup and the initial elevation of the slide, showing that larger runup occurs for subaerial slides than submerged ones. The experimental work of Panizzo, De Girolamo & Petaccia (2005) showed that the duration of underwater landslide motion and the landslide front shape have a major role in determining the maximum wave height. Various numerical studies on the behaviour of tsunamis generated by a three-dimensional sliding mass on a plane beach have been also undertaken (see Liu *et al.* 2005; Lynett & Liu 2005). By studying the free-surface elevation time series for a wide set of numerical simulations for both subaerial and submerged landslides, Lynett & Liu (2005) observed the occurrence of two different wave fields. At the earliest times following the landslide generation, two-dimensional wave motion occurs with high amplitudes only in a small region near the slide. As time passes, these waves then radiate out while fast decaying, while shoreline motion starts to become significant; later, edge waves propagating along the coastline become predominant, while wave amplitudes near the slide become zero. Therefore, since both a shoreline movement and an outgoing wave field are usually induced by the landslide interaction with the water, the study of such transients requires the development of an appropriate two-horizontal-dimension (2HD) model. However, though Liu, Lynett &

https://doi.org/10.1017/S0022112007009731 Published online by Cambridge University Press

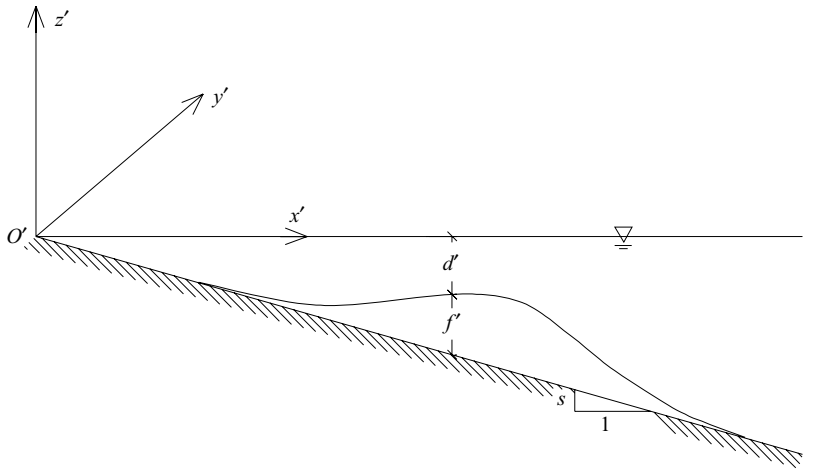


FIGURE 1. The fluid domain in physical coordinates.

Synolakis (2003) developed a one-dimensional (1HD) analytical model, to date very few analytical studies of landslide tsunamis include 2HD effects, as already pointed out by Lynett & Liu (2005).

In §2, an analytical two-horizontal-dimension model of landslide tsunamis is developed based on the forced linear long-wave equation of motion. The above mentioned numerical observations of Lynett & Liu (2005) are then confirmed analytically. In §3 the application of the method of stationary phase enables us to derive a simplified expression for the free-surface elevation at larger times, which consists of propagating transient edge waves. Comparisons with the transient waves due to a displacement of the free surface over a constant depth is made in order to further appreciate the distinctive nature of landslide-generated tsunamis along a sloping beach, which is the absence of a leading wave at large times. In §4 results are discussed; the free-surface elevation time series are analysed and compared to available experimental data. Finally, in §5 the validity of homogeneous models currently used in numerical analysis is discussed.

2. Analytical model

Referring to figure 1, let us consider a straight beach with constant slope s, and define a plane reference system of coordinates (O', x', y'), with the y'-axis along the mean shoreline; water is in the region $x' > 0$. We assume that the landslide originates in a neighbourhood of the origin O', and its shape is symmetric with respect to the y'-axis; the induced wave field is also symmetric in y', allowing us to solve the equation of motion in $y' > 0$ only.

2.1. *Governing equations*

Within the shallow water limit, consider the governing equation for forced long waves on a uniformly sloping beach:

$$\frac{\partial^2 \zeta'}{\partial t'^2} - gs\nabla \cdot (x'\nabla \zeta') = \frac{\partial^2 f'}{\partial t'^2}, \tag{2.1}$$

with g being the acceleration due to gravity, $\nabla(\cdot) = [\partial(\cdot)/\partial x, \partial(\cdot)/\partial y]$ the nabla operator, $\zeta'(x', y', t')$ the free-surface elevation, t' time and $d' = sx' - f'(x', y', t')$

https://doi.org/10.1017/S0022112007009731 Published online by Cambridge University Press

the bottom depth, measured with respect to the mean water level $z' = 0$. In (2.1) $f'(x', y', t')$ is a time-dependent perturbation of the sea floor, representing the landslide moving on the plane beach, as sketched in figure 1. Let H and σ be respectively the maximum vertical thickness and the characteristic horizontal length of the landslide. The following non-dimensional variables can be introduced:

$$x = x'/\sigma, \quad y = y'/\sigma, \quad t = \sqrt{gs/\sigma}\,t', \quad \zeta = \zeta'/H, \tag{2.2}$$

so that the equation of motion (2.1) becomes

$$x\zeta_{xx} + \zeta_x + x\zeta_{yy} = \zeta_{tt} - f_{tt}. \tag{2.3}$$

The subscripts denote derivatives with respect to the relevant variable. We require the free-surface elevation $\zeta(x, y, t)$ to be bounded at the shoreline $x = 0$, and to decay as x tends to infinity for all positive y and t. Since the spatial domain is the quadrant $x > 0$, $y > 0$, and the free-surface elevation is expected to be an even function of y, the cosine Fourier transform of ζ,

$$\hat{\zeta}(x, k, t) = \int_0^\infty \zeta(x, y, t)\cos ky \,\mathrm{d}y, \tag{2.4}$$

can be employed, k being the non-dimensional transform parameter. Equation of motion (2.3) is then transformed into

$$x\hat{\zeta}_{xx} + \hat{\zeta}_x - xk^2\hat{\zeta} = \hat{\zeta}_{tt} - \hat{f}_{tt}. \tag{2.5}$$

By introducing the further transformations

$$\xi = 2kx, \quad \hat{\zeta} = \mathrm{e}^{-\xi/2}Z(\xi, k, t), \tag{2.6a, b}$$

equation (2.5) becomes

$$2k\left[\xi Z_{\xi\xi} + (1-\xi)Z_\xi - \tfrac{1}{2}Z\right] - Z_{tt} = -F_{tt}(\xi, k, t), \tag{2.7}$$

where

$$F(\xi, k, t) = \hat{f}(\xi/2k, k, t)\,\mathrm{e}^{\xi/2}. \tag{2.8}$$

2.2. *Solution*

The transformed equation of motion (2.7) is a non-homogeneous partial differential equation of the second order in the domain $\xi > 0, t > 0$. To obtain its solution, let us first consider the associated homogeneous equation

$$2k\left[\xi Z_{\xi\xi} + (1-\xi)Z_\xi - \tfrac{1}{2}Z\right] - Z_{tt} = 0. \tag{2.9}$$

The solution Z_h of (2.9) can be obtained by means of separation of variables: $Z_h = X(\xi)T(k, t)$. Boundedness of the free surface requires

$$|X(0)| < +\infty, \quad \lim_{x\to\infty} \mathrm{e}^{-\xi/2}X(\xi) = 0. \tag{2.10}$$

Solution of the separated problems for $X(\xi)$ and $T(k, t)$ yields

$$Z_h(\xi, t) = \sum_{n=0}^{\infty} Z_{h_n}(\xi, t) = \sum_{n=0}^{\infty} \mathrm{L}_n(\xi)\left[c_n \cos\omega_n t + d_n \sin\omega_n t\right], \tag{2.11}$$

where $\mathrm{L}_n(\xi) = \mathrm{L}_n^{(0)}(\xi)$ are the Laguerre polynomials, which are orthonormal functions with respect to the weighting function $\mathrm{e}^{-\xi}\xi^a$ in $\xi \in [0, \infty)$:

$$\int_0^\infty \mathrm{e}^{-\xi}\xi^a \mathrm{L}_n^{(a)}(\xi)\mathrm{L}_m^{(a)}(\xi)\,\mathrm{d}\xi = \frac{\Gamma(n+a+1)}{n!}\delta_{nm}, \tag{2.12}$$

https://doi.org/10.1017/S0022112007009731 Published online by Cambridge University Press

Γ being the gamma function, δ_{nm} the Kronecker's operator and a a positive real number; c_n and d_n are to be determined from initial conditions. The relevant eigenvalues are given by

$$\omega_n = \sqrt{k\,(2n+1)}, \quad n = 0, 1, 2, \tag{2.13}$$

which defines the motion eigenfrequencies. The method of variation of parameters can be employed to find the solution of the inhomogeneous problem (2.7) with boundary conditions (2.10). We assume for $Z(\xi, k, t)$ the same algebraic expression as Z_h, i.e.

$$Z(\xi, k, t) = \sum_{n=0}^{\infty} \mathrm{L}_n(\xi) T_n(k, t), \tag{2.14}$$

with T_n unknown functions required to satisfy (2.7). By means of the orthogonality property (2.12), (2.7) yields a differential equation for T_n:

$$T_{n,tt} + \omega_n^2 T_n = \int_0^{\infty} \mathrm{e}^{-\xi} \mathrm{L}_n(\xi) F_{tt}(\xi, k, t)\,\mathrm{d}\xi, \tag{2.15}$$

where the ω_n are still defined by (2.13). We require that at $t = 0$ both the free-surface elevation ζ and velocity $\partial\zeta/\partial t$ are zero; hence $T_n(k, 0) = 0$, $T_{n,t}(k, 0) = 0$. Solution of this initial-value problem gives

$$T_n(k, t) = \frac{2k}{\omega_n} \int_0^{\infty} \mathrm{e}^{-k\alpha} \mathrm{L}_n(2k\alpha) I_n(\alpha, k, t)\,\mathrm{d}\alpha, \tag{2.16}$$

with

$$I_n(\alpha, k, t) = \int_0^t \hat{f}_{\tau\tau}(\alpha, k, \tau) \sin\left[\omega_n (t - \tau)\right] \mathrm{d}\tau. \tag{2.17}$$

Consider a translating Gaussian sea-floor movement, $f(x, y, t) = \exp[-(x - t)^2] s(y)$, where $s(y) = \exp[-(cy)^2]$ is a lateral spreading function and $c = \sigma/\lambda$, λ being the characteristic width of the landslide along the shoreline. Then, the integral function (2.17) can be solved by parts to obtain

$$I_n = \omega_n \hat{s}(k) \left\{ \left[\omega_n a_n - \mathrm{e}^{-\alpha^2}\right] \cos \omega_n t - \left[\frac{2}{\omega_n} \alpha \mathrm{e}^{-\alpha^2} + \omega_n b_n\right] \sin \omega_n t + \mathrm{e}^{-(\alpha - t)^2} \right\}, \tag{2.18}$$

where $\hat{s}(k) = \sqrt{\pi}/(2c) \exp(-k^2/4c^2)$ is the cosine Fourier transform of $s(y)$ and

$$a_n = a_n(\alpha, k, t) = \frac{\sqrt{\pi}}{2} \mathrm{e}^{-\omega_n^2/4} \mathrm{Im} \left\{ \mathrm{e}^{\mathrm{i}\omega_n \alpha} \left[\mathrm{erf}\left(\alpha + \mathrm{i}\frac{\omega_n}{2}\right) - \mathrm{erf}\left(\alpha - t + \mathrm{i}\frac{\omega_n}{2}\right) \right] \right\}, \tag{2.19}$$

while

$$b_n = b_n(\alpha, k, t) = \frac{\sqrt{\pi}}{2} \mathrm{e}^{-\omega_n^2/4} \mathrm{Re} \left\{ \mathrm{e}^{\mathrm{i}\omega_n \alpha} \left[\mathrm{erf}\left(\alpha + \mathrm{i}\frac{\omega_n}{2}\right) - \mathrm{erf}\left(\alpha - t + \mathrm{i}\frac{\omega_n}{2}\right) \right] \right\}. \tag{2.20}$$

$\mathrm{Re}\{\}$ and $\mathrm{Im}\{\}$ are respectively the real and imaginary part of $\{\}$. T_n can now be determined upon substitution of (2.18) into (2.16). Finally, the inverse transform of (2.14), together with the substitutions dictated by (2.6), yields the free-surface elevation

$$\zeta(x, y, t) = \frac{2}{\pi} \sum_{n=0}^{\infty} \int_0^{\infty} \mathrm{e}^{-kx} \mathrm{L}_n(2kx) T_n(k, t) \cos ky\,\mathrm{d}k. \tag{2.21}$$

For a simple physical interpretation of (2.21), define the integral transform $\mathscr{L}^n$ of a given function $u(\alpha, k, t)$ as

$$\mathscr{L}^n\,[u]\,(k, t) = \frac{2k}{\omega_n} \int_0^{\infty} \mathrm{e}^{-k\alpha} \mathrm{L}_n(2k\alpha) u(\alpha, k, t) \mathrm{d}\alpha, \tag{2.22}$$

https://doi.org/10.1017/S0022112007009731 Published online by Cambridge University Press

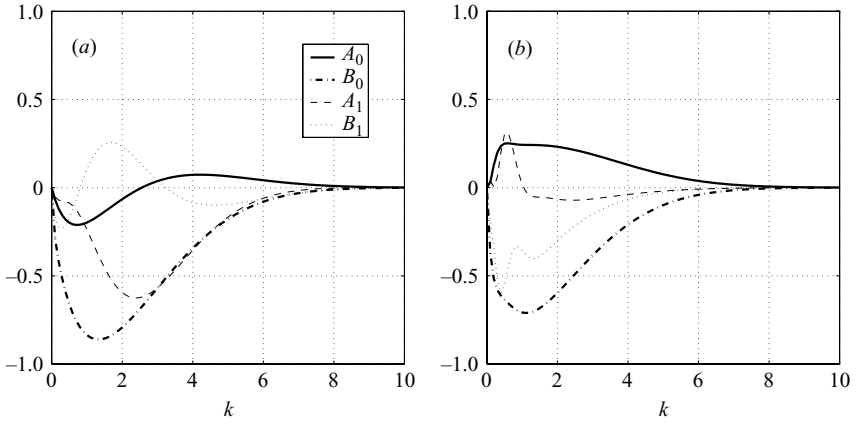


FIGURE 2. Numerical evaluation of A_n and B_n for the first two modes as functions of k; $c = 2$. (*a*) $t = 1$, (*b*) $t = 5$.

so that $T_n = \mathscr{L}^n[I_n]$. Hence, by simply applying the transform $\mathscr{L}^n$ to (2.18) we can formally rewrite (2.21) as $\zeta = \zeta^o + \zeta^e$, where

$$\zeta^o = \frac{2}{\pi}\sum_{n=0}^{\infty}\int_0^{\infty} \mathrm{e}^{-kx}\mathrm{L}_n(2kx)\,[A_n\cos\omega_n t + B_n\sin\omega_n t]\cos ky\,\mathrm{d}k, \tag{2.23}$$

with

$$A_n = A_n(k,t) = \omega_n\hat{s}\mathscr{L}^n\left[\omega_n a_n(\alpha,k,t) - \mathrm{e}^{-\alpha^2}\right], \tag{2.24}$$

$$B_n = B_n(k,t) = -\hat{s}\mathscr{L}^n\left[2\alpha\mathrm{e}^{-\alpha^2} + \omega_n^2 b_n(\alpha,k,t)\right], \tag{2.25}$$

and

$$\zeta^e = \frac{2}{\pi}\sum_{n=0}^{\infty}\int_0^{\infty} \mathrm{e}^{-kx}\mathrm{L}_n(2kx)\,\omega_n\hat{s}\mathscr{L}^n\left[\mathrm{e}^{-(\alpha-t)^2}\right]\cos ky\,\mathrm{d}k. \tag{2.26}$$

Now, ζ^o describes an oscillatory motion in time. Numerical evaluation of (2.24) and (2.25) shows that its coefficients A_n and B_n are fast-decaying functions of k for any given time t, hence the integral in (2.23) is fast convergent in k at all times. The magnitudes of A_n and B_n decrease for increasing n, as can be seen in figure 2. For large t, the second error function in expressions (2.19) and (2.20) tends to unity, and the a_n and b_n in (2.24) and (2.25) do not depend on time. Therefore A_n and B_n approach limiting values that depend only on k.

ζ^e decays exponentially with time. Hence, the landslide generates a twofold wave field made up by oscillatory and evanescent components, the latter rapidly vanishing with time.

2.3. *Time of decay*

To estimate the time of decay of the evanescent term ζ^e, consider (2.26). The $\mathscr{L}^n$ transform inside (2.26) can be approximated by

$$\mathscr{L}^n\left[\mathrm{e}^{-(\alpha-t)^2}\right] \simeq \frac{2k}{\omega_n}\mathrm{e}^{-kt}\mathrm{L}_n(2kt)\int_0^{\infty}\mathrm{e}^{-(\alpha-t)^2}\mathrm{d}\alpha = \frac{\sqrt{\pi}\,k}{\omega_n}(\mathrm{erf}\,t+1)\,\mathrm{e}^{-kt}\mathrm{L}_n(2kt).$$

https://doi.org/10.1017/S0022112007009731 Published online by Cambridge University Press

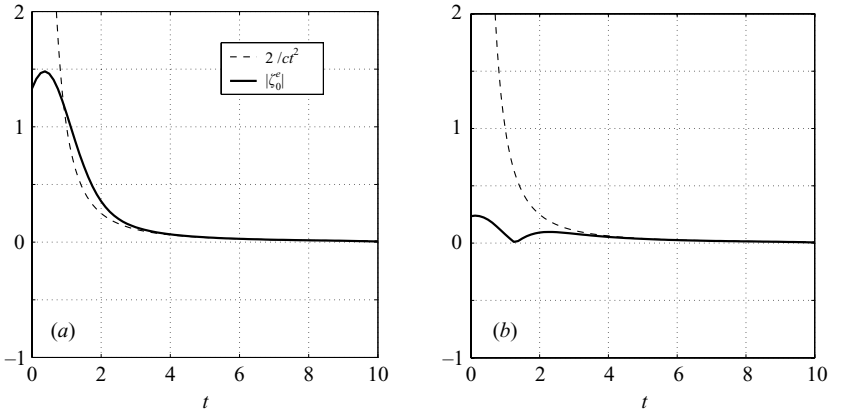


FIGURE 3. Decay of the evanescent term ζ^e for the fundamental mode $n = 0$ at (*a*) $(x, y) = (0, 0)$, (*b*) $(x, y) = (0, 1)$; $c = 2$. Note that for large times $\zeta_0^e \simeq 2/ct^2$.

Therefore, to the crudest approximation, for $t > 1$

$$|\zeta^e| \simeq \left|\zeta_0^e\right| \leqslant \frac{1}{c}(\mathrm{erf}t + 1)\int_0^\infty k\mathrm{e}^{-kt}\,\mathrm{d}k \leqslant \frac{2}{ct^2}, \quad \forall(x, y). \tag{2.27}$$

The evanescent component decays as $O(1/t^2)$ at each point of the fluid domain, as shown in figure 3. Now, define a positive constant $\epsilon \ll 1$. Then $|\zeta^e| \leqslant 2/ct^2 \leqslant \epsilon$ when $t \geqslant t_{dec}$, where

$$t_{dec} = \sqrt{\frac{2}{\epsilon c}} \tag{2.28}$$

is the time of decay of the evanescent component. For $t > t_{dec}$, ζ^e can be neglected, and the free-surface elevation is made up only of the oscillatory component $\zeta \simeq \zeta^o$. As an example, for $\epsilon = 0.05$, $c = 2$, the time of decay is $t_{dec} \simeq 4.5$. With the same order of approximation, (2.28) can be written in physical variables as

$$t'_{dec} \simeq 6.32\sqrt{\frac{\lambda}{gs}}, \tag{2.29}$$

which is similar in form to the characteristic time of motion defined by Watts *et al.* (2003). Relation (2.29) shows that the larger the landslide width λ, the slower the decay of the evanescent component; on the other hand, the steeper the beach, the faster the decay of ζ^e. We next turn to the analysis of ζ^o.

3. Behaviour for large times

Numerical methods have shown that for $t \gg 0$ edge waves are propagating along the shoreline, while the perturbations rapidly diminish near the point of generation O (see Lynett & Liu 2005). To demonstrate this analytically, consider the expression for the nth modal free-surface elevation at the shoreline, $\zeta_n(0, y, t)$. For t large enough to neglect the contribution of the evanescent term ζ^e, the free-surface elevation becomes

$$\zeta_n(0, y, t) \simeq \zeta_n^o(0, y, t) = \frac{2}{\pi}\int_0^\infty [A_n(k, t)\cos\omega_n t + B_n(k, t)\sin\omega_n t]\cos ky\,\mathrm{d}k. \tag{3.1}$$

https://doi.org/10.1017/S0022112007009731 Published online by Cambridge University Press

Let us now consider the integral in (3.1),

$$\frac{2}{\pi}\int_0^\infty A_n \cos\omega_n t\, \cos ky\, \mathrm{d}k = \frac{2}{\pi}\mathrm{Re}\left\{\int_0^\infty A_n \tfrac{1}{2}\left[\mathrm{e}^{\mathrm{i}t(ky/t-\omega_n)} + \mathrm{e}^{\mathrm{i}t(ky/t+\omega_n)}\right]\mathrm{d}k\right\}, \tag{3.2}$$

where the exponential terms represent respectively a right-going wave and a left-going wave. The behaviour of these two waves at large times can be analysed with the method of stationary phase (see Mei, Stiassnie & Yue 2005). For $t \gg 1$, the exponential functions of phase

$$w_n(k) = ky/t \mp \omega_n = ky/t \mp \left[2k\left(n+\tfrac{1}{2}\right)\right]^{1/2} \tag{3.3}$$

oscillate quickly with varying k, sweeping a very small net area, and so determine the integrals in (3.2) to be approximately null. In a neighbourhood of the points $k_n = k_n^*$ where the phase is stationary, the exponential function covers a larger net area, and the integral (3.2) becomes significant. If we denote $\mathrm{d}/\mathrm{d}k() = \dot{()}$, the stationary points for the right-going wave occur at $y/t - \dot{\omega}_n = y/t - C_{g_n} = 0$, where $C_{g_n} = \dot{\omega}_n$ is the nth modal group celerity. Differentiating (3.3) and equating to zero yields $k_n^* = (2n+1)(t/2y)^2$. Note that for the left-going wave there are no stationary points. By Taylor-expanding the phase function w_n about the stationary point k_n^*, the integral (3.2) can be approximated as

$$\frac{2}{\pi}\int_0^\infty A_n(k,t)\cos\omega_n t\, \cos ky\, \mathrm{d}k \simeq \frac{\sqrt{2}A_n(k_n^*,t)}{\left(\pi t|\ddot{\omega}_n(k_n^*)|\right)^{1/2}}\cos\left(k_n^* y - \omega_n t + \frac{\pi}{4}\right), \tag{3.4}$$

with $|\ddot{\omega}_n(k)| = \sqrt{2n+1}/4k^{3/2}$. Analogous considerations can be made for

$$\frac{2}{\pi}\int_0^\infty B_n(k,t)\sin\omega_n t\, \cos ky\, \mathrm{d}k \simeq -\frac{\sqrt{2}B_n(k_n^*,t)}{(\pi t|\ddot{\omega}_n(k_n^*)|)^{1/2}}\sin\left(k_n^* y - \omega_n t + \frac{\pi}{4}\right). \tag{3.5}$$

By substituting (3.4) and (3.5) into (3.1) and summing the single modes, we obtain

$$\begin{aligned}\zeta(0,y,t) &\simeq \sum_{n=0}^{\infty}\zeta_n^o(0,y,t) \simeq \sum_{n=0}^{\infty}\frac{\sqrt{2}}{(\pi t|\ddot{\omega}_n(k_n^*)|)^{1/2}} \\ &\times\left[A_n(k_n^*,t)\cos\left(k_n^* y - \omega_n t + \frac{\pi}{4}\right) - B_n(k_n^*,t)\sin\left(k_n^* y - \omega_n t + \frac{\pi}{4}\right)\right].\end{aligned} \tag{3.6}$$

Equation (3.6) is an approximated expression (error $= O(t^{-1})$, see Mei *et al.* 2005) of the free-surface elevation at the shoreline for large times. In (3.6) each of the modal components is the sum of two waves, of amplitude $\sqrt{2}A_n(\pi t|\ddot{\omega}_n|)^{-1/2}$ and $\sqrt{2}B_n(\pi t|\ddot{\omega}_n|)^{-1/2}$ respectively, both vanishing with time as $t^{-1/2}$.

Finally, by using the same method but for $x > 0$, we obtain the approximated expression for the free-surface elevation for all (x, y) at large times:

$$\zeta(x,y,t) \simeq \sum_{n=0}^{\infty}\mathrm{e}^{-k_n^* x}\mathrm{L}_n\left(2k_n^* x\right)\zeta_n^o(0,y,t). \tag{3.7}$$

Expression (3.7) shows the fast decay in x of the free-surface oscillation, a distinguishing feature of the edge waves. Therefore, at large times the motion consists of a system of edge waves propagating along the shoreline, with amplitudes

https://doi.org/10.1017/S0022112007009731 Published online by Cambridge University Press

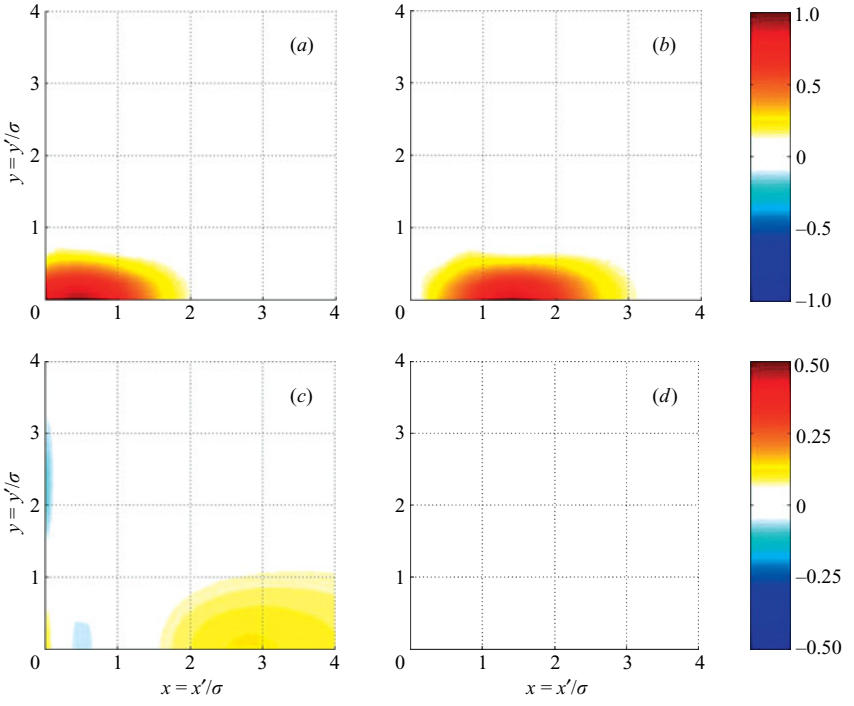


FIGURE 4. Contour levels of the evanescent component ζ^e in non-dimensional variables at times (*a*) $t = 0.5$, (*b*) $t = 1.5$, (*c*) $t = 4.5$, (*d*) $t = 7$. The first six modes have been considered.

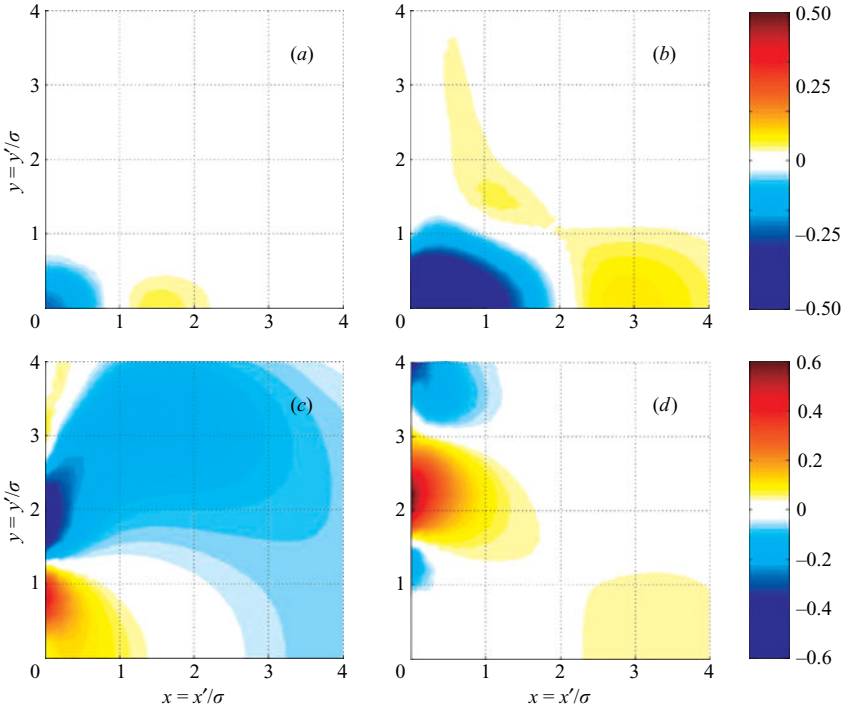


FIGURE 5. Contour levels of the free surface $\zeta = \zeta^e + \zeta^o$ in non-dimensional variables at times (*a*) $t = 0.5$, (*b*) $t = 1.5$, (*c*) $t = 4.5$, (*d*) $t = 7$. The first six modes have been considered.

https://doi.org/10.1017/S0022112007009731 Published online by Cambridge University Press

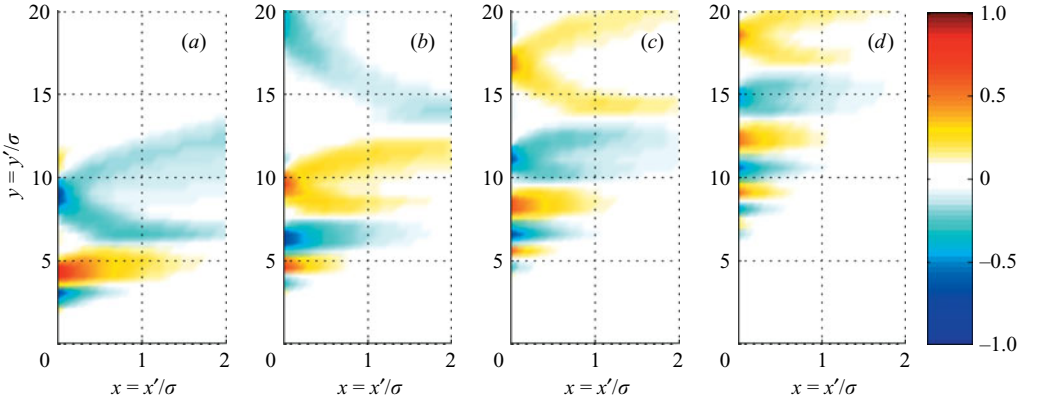


FIGURE 6. Contour levels of the free surface in non-dimensional variables at times (*a*) $t = 10$, (*b*) $t = 15$, (*c*) $t = 20$, (*d*) $t = 30$. The first five modes have been considered.

proportional to $A_n|\ddot{\omega}_n|^{-1/2}$ and $B_n|\ddot{\omega}_n|^{-1/2}$. Note that $|\ddot{\omega}_n|$ increases with no boundaries for decreasing k, causing the above amplitudes to vanish. Hence longer waves, which travel faster since $\dot{\omega}_n = C_{g_n} = (2n+1)/(2\sqrt{k})$, are not those of larger amplitude. This agrees with the results obtained with earlier numerical models and experimental tests (see, for example, Lynett & Liu 2005). The lack of a properly defined leading wave for large times distinguishes landslide-generated tsunamis on a plane beach from transient waves generated and propagating over a constant depth d (see Mei *et al.* 2005; Di Risio & Sammarco 2008). In the latter case, in fact, the dispersion relation $\omega(k) = \sqrt{gk \tanh kd}$ causes the wave amplitude, proportional to $|\ddot{\omega}|^{-1/2}$, to increase as k decreases (i.e. while moving toward the wavefront), till it becomes unbounded at $k = 0$. Solution of this singularity (see Mei *et al.* 2005) yields the known expression for the leading wave in terms of the Airy function. In the present case, instead, there is no singularity at $k = 0$ as discussed above.

4. Discussion

Let us analyse the wave motion generated by a characteristic landslide with parameter $c = \sigma/\lambda = 2$. In figure 4(*a–d*) the contours of the evanescent component ζ^e, expression (2.26), at four different instants are shown. When t is small, ζ^e is non-zero only in a narrow area landward of the slide (see figure 4*a*). After some instants, the evanescent component is propagating mostly in the offshore direction (figure 4*b*), while its amplitude rapidly decreases as t approaches $t_{dec} \simeq 4.5$ (see figure 4*c*). Finally, for $t > t_{dec}$, ζ^e is zero everywhere in the fluid domain (figure 4*d*). Hence the evanescent term is a result of the early interaction between landslide and water, directly affecting the wave motion only during the phase of generation. In this phase, the occurrence of source-specific waves has also been shown via numerical investigation by Lynett & Liu (2005). Now, let us focus on the free-surface elevation $\zeta = \zeta^o + \zeta^e$, given by (2.23) and (2.26), and represented in figure 5(*a–d*). At the earliest times of motion, the landslide pushes water ahead and generates a leading elevation wave. This wave is propagating mostly in the offshore direction, due to the stretched shape of the slide, while propagation along the shore is less noticeable. In the meantime, a depression wave occurs landwards (figure 5*a*). After few instants, the elevation wave is also spreading along the shoreline, while the depression wave dominates over a large area around the origin (figure 5*b*). At larger times the first

https://doi.org/10.1017/S0022112007009731 Published online by Cambridge University Press

elevation wave has left the domain, followed by the propagating depression wave (figure 5*c*). In turn, the latter is wrapping a second elevation wave generated by the elastic rebound at the origin. Water motion along the shoreline becomes evident. Finally, for $t = 7$, the perturbation is travelling mostly in the longshore direction (figure 5*d*), while around the origin the water returns to the unperturbed position. Figure 6(*a–d*) shows four snapshots of the free-surface elevation at large times, and are obtained by using the stationary phase solution (3.7). Starting from the left, note the longshore wave motion being already predominant at $t = 10$ (see figure 6*a*, *b*). By $t = 20$, the wave motion is bounded at the shoreline (figure 6*c*), and later in time only edge waves are present (see figure 6*d*). The first-occurring waves are not those of larger amplitude, as demonstrated in §3. Furthermore, new wave crests are created in the course of propagation, while the perturbation moves ahead from the origin. Longer waves travel faster and are followed by a tail of shorter waves, as obtained numerically by Lynett & Liu (2005). The linear long-wave theory, non-dispersive over bottoms of constant depth, reproduces the dispersive behaviour of the trapped waves over inclined bottoms.

4.1. *Experimental comparison*

In this section the free-surface time series at the shoreline are evaluated and compared to experimental data (see Di Risio *et al.* 2008), obtained by letting an oval block 0.8 m long by 0.4 m wide slide down a steep slope, $s = 0.3$. The landslide centroid is initially positioned at about the free surface, the landslide maximum thickness is 0.05 m, and its maximum cross-sectional area is about 0.03 m^2. The basin is 5.40 m long by 10.8 m wide, 0.8 m deep. By letting our parameters be $\sigma = 0.37$ m, $H = 0.045$ m and $c = 2$, the overall area beneath the forcing function f' approximates the landslide maximum cross-sectional area. In figure 7(*a*, *b*) the free-surface time series at two different points along the shoreline are plotted. The graphs show good correspondence between the theoretical and experimental data. In particular, the overall behaviour of the fluid is reproduced with acceptable accuracy by the model, even though the runups and drawdowns seem to be over-estimated. This happens since the model does not take into account energy dissipation phenomena such as shear actions or wave breaking occurring in the experiment.

5. Approximation with a homogeneous system

So far, the forced initial-value problem set by (2.3), with initial conditions $\zeta = 0$ and $\zeta_t = 0$ at $t = 0$, has been solved. The solution in terms of the free-surface elevation ζ is given by (2.21). For brevity, the above-mentioned initial-value problem will be rewritten as

$$\diamond\zeta = f_{tt}, \quad \zeta(x, y, 0) = 0, \quad \zeta_t(x, y, 0) = 0, \qquad (5.1a, b, c)$$

where $\diamond(\cdot) = -[x(\cdot)_{xx} + x(\cdot)_{yy} + (\cdot)_x - (\cdot)_{tt}]$. It has been argued that (5.1) can be transformed into a simpler homogeneous system, if one considers some approximations in the governing equations and the boundary conditions. First, at $t \simeq t_{dec}$, the landslide has already reached deeper water, so that wave forcing in shallow water is less effective. Also, the initial free-surface perturbation generated by the slide starts to propagate from the shoreline in the horizontal plane (see §4). Therefore, when analysing the behaviour of the system near the shoreline, for $t \geqslant t_{dec}$, the forcing term in (5.1*a*) can be neglected and a homogeneous initial-value problem starting at $t = t_{dec}$ can be considered instead. At this time the

https://doi.org/10.1017/S0022112007009731 Published online by Cambridge University Press

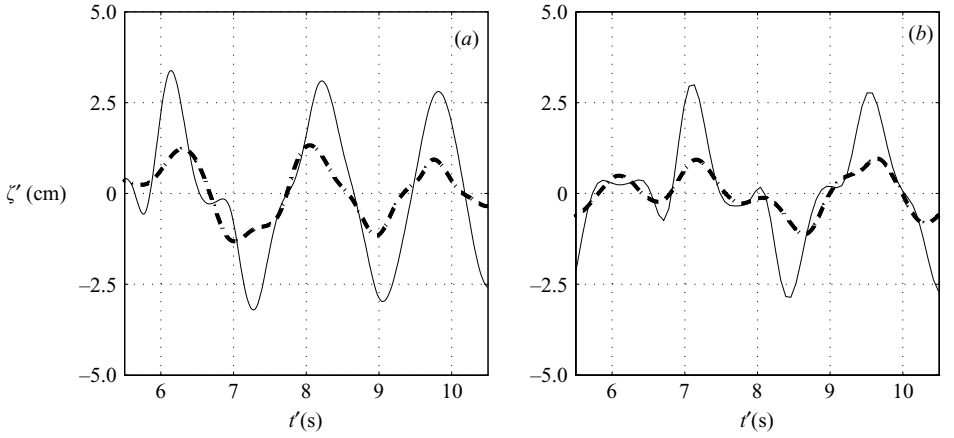


FIGURE 7. Free-surface time series in physical variables at (*a*) $(x', y') = (0, 3.1\text{ m})$, (*b*) $(x', y') = (0, 4.07\text{ m})$. The bold dashed line shows the experimental data (visual imaging technique), the continuous line represents the theoretical values. ζ is evaluated with the stationary phase approximation formula (3.6) and then transformed into dimensional form. The first five modes have been considered.

initial free-surface elevation can be described by a known function of the spatial coordinates, $\zeta(x, y, 0) = g(x, y)$. A double Gaussian function is often used to represent it: $g(x, y) = 2/\pi[\exp(-(x^2 + y^2)) - a\ \exp(-(x^2 + c^2y^2)/b^2)]$, where a and b are shape parameters, depending on the characteristics of the landslide (see Carrier, Wu & Yeh 2003; Watts *et al.* 2005, for a compendium of possible wave forms). Hence to solve the problem, only the initial velocity $\zeta_t(x, y, 0) = h(x, y)$ would need to be set. It has been widely assumed in the literature that after the landslide initiates, the total tsunami energy is almost all potential energy (see Watts *et al.* 2003, 2005). With this hypothesis, the initial velocity can be neglected: $h(x, y) \simeq 0$, and the problem becomes

$$\diamond\zeta = 0, \quad \zeta(x, y, t_{dec}) = g(x, y), \quad \zeta_t(x, y, t_{dec}) = 0, \quad t \geqslant t_{dec}, \qquad (5.2a, b, c)$$

i.e. a non-forced homogeneous initial-value system. This approach is currently employed in some landslide-generated-tsunami forecasting models (see Watts *et al.* 2003).

Here we further investigate the analytical effectiveness of describing the fundamental behaviour of the fluid in this manner. In so doing, the following questions are posed: does a homogeneous system equivalent to (5.1) really exist, and, for $t \geqslant t_{dec}$, is this system (5.2)? In order to respond to the first question, define a function $\eta(x, y, t - \tau)$, with τ a positive real parameter, solution of

$$\diamond\eta = 0, \quad \eta(x, y, 0) = 0, \quad \eta_t(x, y, 0) = f_{tt}(x, y, \tau), \quad t \geqslant \tau\ . \qquad (5.3a, b, c)$$

This is a homogeneous system, starting at $t = \tau$, with zero initial free-surface elevation and initial velocity given by the forcing term $f_{tt}(x, y, \tau)$. Extension of Duhamel's principle to the forced problem (5.1) reveals that

$$\zeta(x, y, t) = \int_0^t \eta(x, y, t - \tau)\, \mathrm{d}\tau \qquad (5.4)$$

is the solution of (5.1). Hence the first question has a positive answer: the homogeneous system (5.3), together with Duhamel's integral formula (5.4), yield

https://doi.org/10.1017/S0022112007009731 Published online by Cambridge University Press

the solution of (5.1). No other equivalent homogeneous systems seem to exist. For a practical numerical simulation, solution (5.4) could be more suitable than directly solving the forced system (5.1). Now the second question: the equivalence between (5.1) and (5.2). Consider again the full problem (5.1), but with initial time $t = t_{dec}$:

$$\diamond\zeta = f_{tt}(x, y, t), \quad \zeta(x, y, t_{dec}) = \bar{g}(x, y), \quad \zeta_t(x, y, t_{dec}) = \bar{h}(x, y), \qquad (5.5a, b, c)$$

where, taking only ζ^o,

$$\bar{g} = \frac{2}{\pi}\sum_{n=0}^{\infty}\int_0^{\infty} \mathrm{e}^{-kx}\mathrm{L}_n(2kx)\,[A_n(k, t_{dec})\cos\omega_n t_{dec} + B_n(k, t_{dec})\sin\omega_n t_{dec}]\cos ky\,\mathrm{d}k, \qquad (5.6)$$

$$\bar{h} = \frac{2}{\pi}\sum_{n=0}^{\infty}\int_0^{\infty} \mathrm{e}^{-kx}\mathrm{L}_n(2kx)\omega_n\{[A_{n,t} + \omega_n B_n]_{t=t_{dec}}\cos\omega_n t_{dec} + [B_{n,t} - \omega_n A_n]_{t=t_{dec}} \times \sin\omega_n t_{dec}\}\cos ky\,\mathrm{d}k. \qquad (5.7)$$

Equations (5.6) and (5.7) are respectively the free-surface elevation and velocity at $t = t_{dec}$ computed with (2.23). By definition, for $t \geqslant t_{dec}$ a rigorous analytical equivalence occurs only between systems (5.1) and (5.5). The latter is equal to (5.2) if and only if: (i) the forcing term f_{tt} is omitted, (ii) the initial free-surface elevation (5.6) is substituted with the easier double Gaussian form $g(x, y)$, (iii) the initial velocity (5.7) is neglected. As discussed above, point (i) might not produce appreciable errors in shallow water. On the other hand, the approximations in points (ii) and (iii) might result in simulating a different physical behaviour of the system. In particular, the total neglect of the initial velocity seems to have no analytical confirmation, since it cannot be stated that (5.7) is zero in all the fluid domain for any shape of the landslide (i.e. for any t_{dec}). In conclusion, no analytical demonstration of the correctness of replacing the homogeneous problem (5.2) in place of (5.1) seems to exist. The usage of a homogeneous system instead of the forced one has an analytical confirmation only within Duhamel's integral representation (5.4).

6. Conclusion

An analytical forced two-horizontal-dimension model has been developed to analyse the distinguishing physical features of landslide-induced tsunamis along a straight coast. After a short transient immediately following the landslide generation, the wave motion starts to be trapped at the shoreline and finally only transient longshore travelling edge waves are present. Longer waves travel faster and are followed by a tail of shorter waves, while new crests are created. Unlike transient waves generated and propagating in water of constant depth, for landslide-induced tsunamis along a sloping beach the larger waves are not in the front of the wavetrain, but are shifted toward the middle of it. Experimental comparison shows the validity of the model in reproducing the physical behaviour of the system. Finally, the accuracy of homogeneous initial-value models in reproducing landslide-generated tsunamis is discussed. Since no analytical demonstration of the validity of this approach seems to exist, usage of such simplified models is advised only for quick runup assessment.

Experimental data provided by Dr M. Di Risio have been very useful for experimental comparison. Fruitful discussions and suggestions of Dr A. Panizzo and Dr G. Bellotti are also kindly acknowledged. Significant contribution from Professor P. Lynett has been a powerful engine for further insight into the problem.

https://doi.org/10.1017/S0022112007009731 Published online by Cambridge University Press

REFERENCES

Carrier, G. F., Wu, T.-R. & Yeh, H. 2003 Tsunami run-up and draw-down on a plane beach. *J. Fluid Mech.* **475**, 79–99

Di Risio, M., Bellotti, G., Panizzo, A. & De Girolamo, P. 2008 Three-dimensional experiments on water waves generated by landslides at a sloping coast. *J. Fluid Mech.* (submitted).

Di Risio, M. & Sammarco, P. 2008 Transient linear waves generated by a falling box. *J. Waterway, Port, Coastal Ocean Engng*., **134**, (in press).

Liu, P. L.-F., Lynett, P. & Synolakis C. E. 2003 Analytical solutions for forced long waves on a sloping beach. *J. Fluid Mech.* **478**, 101–109.

Liu, P. L.-F., Wu, T.-R., Raichlen, F., Synolakis, C. E. & Borrero, J. C. 2005 Runup and rundown generated by three-dimensional sliding masses. *J. Fluid Mech.* **536**, 107–144.

Lynett, P. & Liu, P. L.-F. 2005 A numerical study of the runup generated by three-dimensional landslides. *J. Geophys. Res.* **110**, C03006.

Mei, C. C., Stiassnie, M. & Yue, D. 2005 *Theory and Application of Ocean Surface Waves*. World Scientific.

Panizzo, A., De Girolamo, P. & Petaccia, A. 2005 Forecasting impulse waves generated by subaerial landslides. *J. Geophys. Res.* **110**, C12025.

Watts, P. 1997 Water waves generated by underwater landslides. PhD thesis, California Institute of Technology.

Watts, P., Grilli, S. T., Kirby, J. T., Fryer, G. J. & Tappin, D. R. 2003 Landslide tsunami case studies using a Boussinesq model and a fully nonlinear tsunami generation model. *Nat. Hazard. Earth Syst. Sci.* **3**, 391–402.

Watts, P., Grilli, S. T., Tappin, D. R. & Fryer, G. J. 2005 Tsunami generation by submarine mass failure. II: predictive equations and case studies. *J. Waterway, Port, Coasal Oc. Engng*. **131**, 298–310.

Wiegel, R. L. 1955 Laboratory studies of gravity waves generated by the movement of a submerged body. *Trans. Am. Geophys. Union* **36**, 5.

https://doi.org/10.1017/S0022112007009731 Published online by Cambridge University Press